Origin of Low Sensitizing Efficiency of Quantum Dots in Organic Solar Cells

Sybren ten Cate, Juleon M. Schins,* and Laurens D. A. Siebbeles*

Optoelectronic Materials Section, Department of Chemical Engineering, Delft University of Technology, Julianalaan 136, 2628 BL Delft, The Netherlands.

ABSTRACT Organic semiconductors are of great interest for application in cheap and flexible solar cells. They have a typical absorption onset in the visible. Infrared light can be harvested by use of lead-chalcogenide quantum dot sensitizers. However, bulk-heterojunction solar cells with quantum-dot sensitizers are inefficient. Here we use ultrafast transient absorption and time-domain terahertz spectroscopy to show that charge localization on the quantum dot leads to enhanced coulomb attraction of its counter charge in the organic semiconductor. This localization-enhanced coulomb attraction is the fundamental cause of the poor efficiency of these photovoltaic architectures. It is of prime importance for improving solar cell efficiency to directly photogenerate spatially separated charges. This can be achieved when both charges are delocalized. Our findings provide a rationalization in the development of photovoltaic architectures that exploit quantum dots to harvest the near-infrared part of the solar spectrum more efficiently.

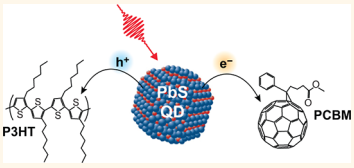

KEYWORDS: quantum dot · organic semiconductor · bulk heterojunction · infrared photovoltaic · ultrafast spectroscopy · terahertz spectroscopy

Currently, there is a great interest in the development of cheap, solution-processable organic materials for application in photovoltaic devices.[1,2] In this context, conjugated polymers as light absorbers with fullerene derivatives as electron acceptors are attracting a great deal of attention.[3,4] Unfortunately, the near-infrared (NIR) portion of the solar spectrum remains largely unabsorbed by these materials. The spectral sensitivity can be extended by including lead-chalcogenide quantum dots (QDs) as sensitizers, which have a high absorption coefficient with an onset that can be tuned throughout the NIR by variation of their size.[5] Indeed, it was recently concluded that electrons and holes can be extracted from excited PbS-oleate QDs in a bulk heterojunction (BHJ) with the fullerene derivative [6,6]-phenyl-C_{61}-butyric acid methyl ester (PCBM) and the conjugated polymer regioregular poly(3-hexylthiophene) (P3HT).[6,7] However, the NIR power-conversion efficiency of QD-sensitized BHJ photovoltaics remains orders of magnitude lower than that of either fully organic or fully QD-based devices.[8] The poor performance of a BHJ containing spherical QDs may be due to inefficient charge separation. The latter has been associated with the nanoparticle shape, and it was demonstrated that the charge separation efficiency increases when going from spherical QDs to rods or tetrapods.[9] Another way of achieving efficient charge separation is by creating a layer of linked spherical QDs.[8,10,11]

The question remains why BHJ photovoltaics comprising lead-chalcogenide QDs, a conjugated polymer, and/or PCBM have a poor NIR power-conversion efficiency. In this paper we aim to explain the poor performance of lead-chalcogenide QDs as NIR sensitizers in BHJ photovoltaics. This is achieved by quantifying the efficiency of charge transfer by means of ultrafast transient absorption spectroscopy measurements (TA) and by measuring the mobility of the charges using ultrafast time-resolved terahertz spectroscopy (THz);[12,13] see Methods. Combined use of these two experimental techniques on a series of samples of different composition enables a direct characterization of charge-carrier behavior. Charge transfer from photoexcited PbS QDs to the organic material components was found to occur; however, the charges produced in this way have a negligible mobility compared to those produced in a fully organic BHJ. We conclude this to be due to coulomb attraction between the charge transferred from a QD and the remaining opposite charge that is localized on a single QD. Thus we reach a general finding that explains the data presented here and other literature data.

RESULTS AND DISCUSSION

The PbS QDs studied in this work have an average diameter of 2.5 nm and contain oleic acid as passivating surface ligand,

* Address correspondence to j.m.schins@tudelft.nl; l.d.a.siebbeles@tudelft.nl.

Received for review July 9, 2012 and accepted September 5, 2012.

Published online September 05, 2012
10.1021/nn303058u

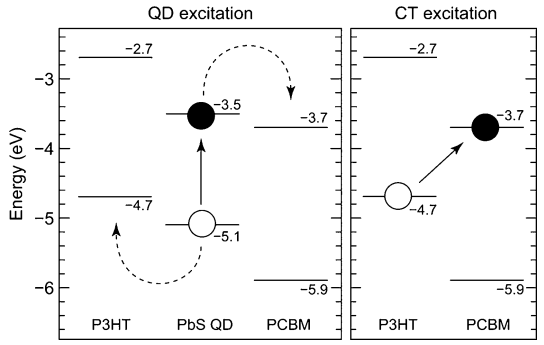

Figure 1. Energy diagram showing HOMO and LUMO levels of PbS QDs[5] of the size as studied and P3HT and PCBM.[35] Electron transfer to PCBM and hole transfer to P3HT (dashed arrows) is energetically feasible from a photoexcited PbS QD. Excitation of the charge-transfer (CT) state, in which an electron is transferred from the P3HT HOMO to the PCBM LUMO, is also possible at our excitation wavelength. The P3HT levels depend on P3HT crystallinity,[36] which may differ in the proximity of QDs.

similar to earlier device and spectroscopic studies.[6,7,14] The first optical absorption peak is at 780 nm. It is inferred from the long photoluminescence lifetime that charge trapping at surface defects is negligible (Figure S1). The small PbS QD size ensures a favorable driving force for electron transfer[15] from a photoexcited PbS QD to PCBM and hole transfer to P3HT in π-stacked domains (*cf.* Figure 1). A pure QD film and BHJs of PbS QDs with P3HT and/or PCBM and of P3HT with PCBM were prepared by drop-casting from solution with equal weight fraction of each material. The optical absorption spectra of the BHJs exhibit a clearly discernible optical absorption peak due to PbS QDs with the band gap being retained upon blending (Figure S2).

Quantum Yields of Charge Transfer. Ultrafast optical pump−probe spectroscopy was used to determine the yields of charge transfer from photoexcited PbS QDs to PCBM and P3HT (see Methods). Both pump and probe laser pulses were centered at 800 nm in order to photoexcite and probe excitons or excess charges at the band gap of our PbS QDs. Figure 2a shows the transient change of the optical absorption cross section per absorbed pump photon, $\bar{\sigma} \equiv \Sigma_i \phi_i \Delta\sigma_i$ (see Methods), with ϕ_i being the quantum yield for photogeneration of species *i* and $\Delta\sigma_i$ the change in absorption cross section due to this species.

The change in absorption cross section at the band gap of the PbS QDs due to the presence of excitons or excess charges was obtained from a TA measurement on a neat film of PbS QDs (solid black curve, Figure 2a). An exciton in a PbS QD results in a reduced ground-state absorption due to the presence of a hole and stimulated emission from the excited electron. The bleach at the band gap is determined by state-filling effects, within the approximation that transition strengths are not affected by a spectator charge. In this case, the cross sections for bleach, $\Delta\sigma_{PbS}$, of the

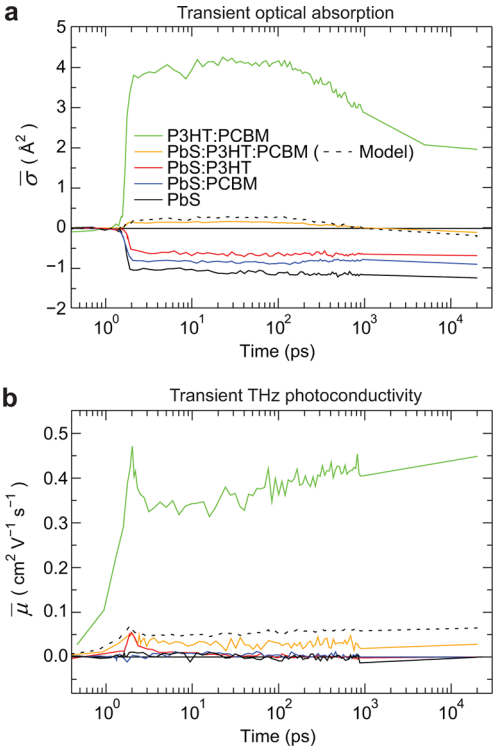

Figure 2. Time-resolved spectroscopic data of four BHJs of different composition and a pure PbS QD film. (a) Transient change of optical absorption per absorbed excitation photon. The vertical axis displays the weighted mean of the changes in cross section associated with the photogenerated species: $\bar{\sigma} \equiv \Sigma_i \phi_i \Delta\sigma_i$ (see Methods). (b) Time-resolved terahertz conductivity per absorbed excitation photon. The vertical axis displays the weighted mean of the charge mobilities: $\bar{\mu} \equiv \Sigma_i \phi_i \mu_i$ (see Methods). Color coding as in panel "a". From comparing results (dashed) of a simple model (see text) with the ternary blend data (yellow) we conclude that charges transferred from QDs have negligible mobility.

electron and hole are equal. This is found to agree with experiment.[16] Therefore, the initial bleach is given by $\bar{\sigma}_{PbS} = 2\Delta\sigma_{PbS}$. The amplitude of the TA transient of the PbS QD film yields $\Delta\sigma_{PbS} = -0.51 \pm 0.02$ Å^2 (standard error of mean, SEM). The optical bleach exhibits no decay on the time scale of 20 ns, in agreement with the long exciton lifetime of 1.5 μs in solution (Figure S1), from which we infer an absence of exciton decay at defects. Interestingly, the bleach of the PbS QD film appears to slightly increase during time, which is attributed to energetic relaxation of excitons by diffusion to larger QDs with a smaller band gap and larger cross section for optical bleach.

Photoexcitation of the charge-transfer state (CT) in the P3HT:PCBM BHJ at 800 nm leads to promotion of a valence electron from the highest occupied molecular orbital (HOMO) of P3HT to the lowest unoccupied molecular orbital (LUMO) of PCBM.[17] The TA probed at 800 nm (green curve, Figure 2a) is due to the $P3HT^+$ cation only, since at this wavelength the $PCBM^-$ anion does not give a change in optical transmission.[18−20] The initial magnitude of the TA is equal to the cross

section for absorption by $P3HT^+$; *i.e.*, $\bar{\sigma}_{P3HT:PCBM} = \Delta\sigma_{P3HT^+} = 3.9 \pm 0.1$ Å^2 (SEM). The decay of the TA after 100 ps is due to geminate electron−hole recombination, while the remaining absorption for times exceeding a few nanoseconds is due to free charges that decay on a millisecond time scale.[18]

The optical cross sections, as determined above, are used below to obtain the quantum yields of charge transfer from photoexcited PbS QDs to PCBM and P3HT from TA measurements on BHJs.

The TA for the PbS:PCBM BHJ (blue curve, Figure 2a) is less negative than that for the PbS QD film, which is due to electron transfer from photoexcited PbS QDs to PCBM. The amplitude of the bleach for the PbS:PCBM BHJ is determined by excitons in PbS QDs that have not undergone charge transfer and holes remaining in a PbS QD after electron transfer to PCBM with quantum yield ϕ_e; *i.e.*, $\bar{\sigma}_{PbS:PCBM} = (2 - \phi_e)\Delta\sigma_{PbS}$. The amplitude of the TA for the PbS:PCBM BHJ ($\bar{\sigma}_{PbS:PCBM} = -0.81 \pm 0.02$ Å^2, SEM) and the value of $\Delta\sigma_{PbS}$ determined above result in $\phi_e = 0.41 \pm 0.06$ (SEM). The step-like kinetic behavior implies that electron transfer takes place within ∼100 fs, while charge recombination occurs on times exceeding 20 ns. The high rate for electron transfer from a photoexcited PbS QD to PCBM can be understood on the basis of the classical Marcus rate for electron transfer,[21] given by $k = 2\pi J^2/[\hbar(4\pi\lambda k_B T)^{1/2}] \exp[-(\Delta G + \lambda)^2/(4\lambda k_B T)]$, with J being the electronic coupling matrix element, $\hbar$ the reduced Planck constant, λ the reorganization energy, ΔG the driving force, k_B the Boltzmann constant, and T the temperature. Figure 1 shows that $\Delta G = -0.2$ eV, which is close to the negative of the reorganization energy involved in electron transfer to a PCBM molecule,[22] so that $\Delta G + \lambda$ is negligible and the Marcus rate is close to optimal. To obtain a transfer rate exceeding $(100\text{ fs})^{-1}$ for $\lambda = 0.2$ eV, the electronic coupling must be $J > 16$ meV, which is not particularly high for charge transfer between organic molecules.[23] Hence, the high rate for electron transfer in the present system stems from (near) cancellation of ΔG and λ.

The amplitude of the TA change for the PbS:P3HT BHJ (red curve, Figure 2a) is less negative than for the PbS QD film, which is attributed to reduced bleach due to hole transfer from photoexcited PbS QDs to P3HT and induced absorption by $P3HT^+$. The step-like kinetic behavior implies that hole transfer occurs promptly within 100 fs, while charge recombination plays no role on the 20 ns time scale. The absence of decay implies that charge recombination is slower than 20 ns. The amplitude of the transient of the PbS:P3HT BHJ is given by $\bar{\sigma}_{PbS:P3HT} = (2 - \phi_h)\Delta\sigma_{PbS} + \phi_h\Delta\sigma_{P3HT^+}$, where ϕ_h is the quantum yield for hole transfer. Using the cross sections for bleach due to a charge in a PbS QD and absorption by $P3HT^+$, it is found that $\phi_h = 0.091 \pm 0.008$ (SEM). This value agrees with the internal quantum efficiency range of 5−11% found for a PbS-butylamine:P3OT photovoltaic device upon illumination with 720 nm light.[24] The quantum efficiency for hole transfer to P3HT is lower than for electron transfer to PCBM, in agreement with earlier results.[6] The low quantum yield for hole transfer is likely due to limited interfacial contact between P3HT chains and the PbS QD surface that contains bulky oleic acid capping molecules. In addition, local structural disorder in the form of kinks and torsions along a P3HT chain enhances the ionization potential, which may cause the driving force for hole transfer to become energetically unfavorable.

For the ternary PbS:P3HT:PCBM BHJ a fraction $X = 0.86$ (see Supplementary Note 1 in the SI) of the absorbed 800 nm pump photons causes excitation of PbS QDs, while the remaining fraction of absorbed photons promotes an electron from the HOMO of P3HT to the LUMO of PCBM. The TA for the ternary BHJ (yellow curve, Figure 2a) exhibits absorption at shorter times followed by a small bleach at longer times. The absorption at short times is due to a dominant contribution of $P3HT^+$, while at longer times charges or excitons in PbS QDs dominate to give a net bleach. The crossover from absorption to bleach of the ternary BHJ occurs after ∼1 ns, which is the same time scale as the geminate charge recombination in the P3HT:PCBM BHJ (green curve) and can thus be attributed to reduction of absorption by $P3HT^+$. Indeed, the dashed black curve in Figure 2a shows that the TA of the ternary BHJ can to a good approximation be reproduced by a linear combination of the decaying transient for the P3HT:PCBM BHJ (green curve) and a step-like contribution due to initial photoexcitation of PbS QDs (solid black curve); $\bar{\sigma}_{PbS:P3HT:PCBM}(t) = (1 - X)\bar{\sigma}_{P3HT:PCBM}(t) + X[(2 - \phi_e - \phi_h)\Delta\sigma_{PbS} + \phi_h\Delta\sigma_{P3HT^+}(t)]$. The transient composed in this way (dashed black curve) agrees with that measured for the ternary BHJ (yellow curve) to within the expected uncertainty of ±0.05 Å^2 (SEM). This implies that the quantum yields for electron and hole transfer from PbS QDs in the ternary and binary BHJs are comparable.

Mobility of Charges. The mobility of charges was investigated by time-domain THz photoconductivity measurements. The sample is photoexcited by a laser pulse centered at 800 nm, and the attenuation of the THz electric field waveform is measured as a function of delay time. This yields the sum of the products of the quantum yield for generation of charges of type i and their mobility μ_i; *i.e.*, $\bar{\mu} \equiv \Sigma_i\phi_i\mu_i$ (see Methods). This quantity is presented in Figure 2b as a function of pump−probe delay time for different BHJs.

The THz photoconductivity of the P3HT:PCBM BHJ (green curve, Figure 2b) is predominantly due to photoexcitation of an electron from the HOMO of P3HT to the LUMO of PCBM and to a small extent to photoexcitation of P3HT.[17,25] The generation of mobile charges by excitation of the CT state is understood in terms of immediate charge delocalization.[26,27]

The ultrafast decay of the photoconductivity within ~1 ps may be due to relaxation of the charge mobility resulting from coupling with nuclear vibrations (polaron formation) and possibly recombination of electrons and holes that are generated within a P3HT domain. The initial decay is followed by a rise of the photoconductivity, which may be due to relaxation of charges into more ordered domains where the mobility is higher, or possibly may result from separation of electrons and holes out of their coulomb attraction. However, our following conclusions are independent of the interpretation of this rise and only require the combined electron and hole mobility value at a single, arbitrarily chosen pump−probe delay time. Taking this time directly after the initial relaxation, the sum of the electron and hole mobility is found to be $\mu_e + \mu_h = 0.34 \pm 0.01$ cm^2 V^{-1} s^{-1} (SEM). This is used as a reference value for comparison with the mobilities of charges in the PbS-QD-containing BHJs.

As expected, the photoconductivity of the PbS QD film (black curve, Figure 2b) is negligible due to the bulky oleic acid surface ligands, leading to larger interdot distances and smaller electronic coupling between QDs. For the PbS:PCBM BHJ (blue curve) the product of the quantum yield for electron transfer and the electron mobility is $\phi_e\mu_e < 3 \times 10^{-3}$ cm^2 V^{-1} s^{-1}, with the upper limit determined as the sum of the mean and standard error. For the PbS:P3HT BHJ (red curve) it is found that $\phi_h\mu_h < 5 \times 10^{-4}$ cm^2 V^{-1} s^{-1}. Using the quantum yields determined from the TA data, the mobilities of electrons and holes originating from PbS QDs are determined to be $\mu_e < 7 \times 10^{-3}$ cm^2 V^{-1} s^{-1} and $\mu_h < 5 \times 10^{-3}$ cm^2 V^{-1} s^{-1}. These values are significantly smaller than microwave mobilities of electrons and holes in a P3HT:PCBM BHJ.[28] In agreement with this, the sum of the THz mobilities of electrons and holes originating from charge transfer from a photoexcited PbS QD is almost 30 times smaller than for direct charge generation within a P3HT:PCBM BHJ. Such an effect is also found for the ternary PbS:P3HT:PCBM BHJ. The fraction of absorbed photons within a P3HT:PCBM domain (CT excitation of an electron from the HOMO of P3HT to the LUMO of PCBM; see Figure 1) is given by $(1 - X) = 0.14$. Scaling of the THz photoconductivity transient for P3HT:PCBM with this fraction overestimates the THz transient for the ternary BHJ; see dashed black curve in Figure 2b. Hence, those charges that are generated *via* photoexcitation of PbS QDs do not significantly contribute to the THz photoconductivity. Furthermore, the average mobility of charges directly generated in a P3HT:PCBM domain *via* CT excitation is negatively affected by the presence of QDs in the ternary blend. A uniformly increased value of the dielectric constant of the blend would decrease the coulomb interaction and hence increase the charge mobility. However, the local increase of the dielectric constant due to the PbS QDs may work as a localizing agent for charges in P3HT:PCBM, as these may be attracted to their induced image charge. Furthermore, charges may also become localized in the vicinity of an oppositely charged QD. The localization of charges in P3HT:PCBM around PbS QDs leads to restricted charge motion.

CONCLUSION AND IMPLICATIONS

We infer that charge transfer from a PbS QD in a BHJ with PCBM or P3HT leads to a charge localized within a QD and a counter charge in the organic material. The localized charge in a QD coulombically attracts the counter charge in the organic material, which strongly reduces its mobility and ability to escape from eventual recombination. This finding allows additional understanding of literature observations. The inefficient operation of a photovoltaic device based on a BHJ consisting of CdSe QDs and P3HT was previously attributed to fast electron trapping at QD defects.[29] According to the present work the device efficiency will be limited by the coulomb interaction between the electron on a CdSe QD and the hole in P3HT, even in the absence of charge trapping at QD defects. Recently, it was found that an external electric field is needed to obtain an appreciable photocurrent from an NIR-sensitive photodiode based on a ternary BHJ identical to that in the present work.[14] According to the findings from the current study, the external electric field is needed to separate coulombically bound geminate charge pairs. An interesting observation from the literature is that the NIR power-conversion efficiency of photovoltaic devices based on a BHJ of lead-chalcogenide QDs and an organic charge acceptor is orders of magnitude lower than for devices based on an organic BHJ or a QD film.[8] The efficient operation of QD films is hereby rationalized, since the strong coupling between QDs allows for charge delocalization and separation of opposite charges. Charge delocalization plays the important role of increasing the effective separation between geminate charges, thereby reducing coulomb attraction.

METHODS

Quantum-Dot Synthesis and Quality Determination. Small PbS-oleate QDs were synthesized[30,31] with a mean diameter of 2.5 ± 0.1 nm (standard deviation, SD) as inferred from the central wavelength of the first absorption peak, using an empirical sizing relation[32] (the accuracy of which has been confirmed for small QDs[37]). Chemicals used are listed in Supplementary Note 3.

Sample Preparation. Blend solutions were prepared by weighing PbS QDs, P3HT, and PCBM under ambient conditions (small PbS QDs are air stable[37]) and adding the solvent mixture (9:1 chloroform/chlorobenzene by volume) under inert gas to result in a QD concentration of 5 mg mL^{-1}. The solutions were magnetically stirred overnight at room temperature. One series of films was drop cast for measurements of optical absorption

spectra under ambient conditions. A second film series was prepared for transient absorption and THz spectroscopy under N_2 atmosphere to ensure sample stability. The solutions were desiccated in a glovebox to remove oxygen, redispersed in the solvent mixture, and again stirred overnight. Films were drop cast and continually kept under N_2. Quartz substrates and magnetic stirrers were ultrasonically cleaned in two 10-minute cycles: one with ethanol, followed by one with hexane. Drop casting was performed in a glovebox and on a level surface. Per substrate, 100 μL of solution was deposited and allowed to slowly dry. After the films had dried under atmospheric pressure, they were left under vacuum for 1 h to ensure that all solvents were removed.

Sample Stability. QDs in PCBM-containing BHJs required a low-oxygen atmosphere during laser excitation in order to avoid a blue shift of the QD band gap absorption peak. We ascribe the blue shift to an oxidation of the outer layers of the QD by singlet oxygen, which is likely produced by PCBM upon photoexcitation, since C_{60} is known to be a potent generator of singlet oxygen.[38]

Transient-Absorption Spectroscopy. BHJs were photoexcited and probed using pulses from a Ti:Sapphire chirped-pulse amplified laser system (Libra-USP-HE, Coherent Inc.) running at 1.5 kHz, delivering <50 fs, 3.5 mJ pulses with a central wavelength of 800 nm. The probe beam was imaged onto a silicon PIN photodiode (Vishay BPW34). The pump was spatially separated from the probe downstream of the sample, and orthogonal polarization of the beams allowed further separation by means of a polarizer. The incident pump fluence of 4.4×10^{13} photons cm^{-2} was found to be sufficiently low for higher-order interactions between excitons or charges to be insignificant. For small changes in absorption cross section, the normalized change in optical transmission due to photoexcitation of the sample is

$$\bar{\sigma} \equiv -\frac{T_{on} - T_{off}}{T_{off} I_0 F_A} = -\frac{1}{I_0 F_A}\left[\exp\left(-L\sum_i N_i \Delta\sigma_i\right) - 1\right]$$

$$\approx \frac{L}{I_0 F_A}\sum_i N_i \Delta\sigma_i = \sum_i \varphi_i \Delta\sigma_i \quad (1)$$

where T_{on} is the transmission through the sample in the excited state, T_{off} is the transmission through the sample in the ground state, I_0 is the incident fluence, F_A is the fraction of incident light absorbed by the sample, L is the film thickness, N_i is the volume number density of excited species i, $\Delta\sigma_i$ is the change in the absorption cross section associated with excited species i, and $\phi_i = N_i L/I_0 F_A$ is the quantum yield of excited species i. Hence, $\Delta\sigma_i > 0$ for photoinduced absorption of probe light and $\Delta\sigma_i < 0$ for enhanced transmission of probe light due to stimulated emission and/or ground-state bleach.

Time-Domain Terahertz Spectroscopy. The ultrafast photoconductivity of samples was measured by time-domain terahertz photoconductivity. In this technique, the probe pulse is an electric field waveform of picosecond duration in the terahertz frequency range. Interaction with mobile charge carriers in the photoexcited sample leads to absorption of the probe to an extent that is determined by the conductivity. This experimental technique is detailed elsewhere.[12,13] Samples were photoexcited with a <50 fs laser pulse from the laser described above and probed by a picosecond terahertz pulse. Terahertz pulses were generated by optical rectification in a ZnTe crystal. The excitation beam (diameter 5 mm) was aligned on the sample with the focused terahertz beam (diameter <2 mm). The terahertz field transmitted through the samples was detected by means of the Pockels electro-optic effect in a 0.5 mm ZnTe crystal. The incident fluence was taken as 1.17×10^{15} photons cm^{-2} for all samples. This fluence was found to be sufficiently low for linear response (*i.e.*, absence of second or higher order decay of charges or excitons). The product of the quantum yield of charge-carrier photogeneration, ϕ_i, and the mobility, μ_i, summed over all charge carrier species i, is related to the change in the transmission of electric field at the maximum of the terahertz waveform as[12,33]

$$\bar{\mu} \equiv \sum_i \varphi_i \mu_i = -\frac{2nc\varepsilon_0}{e}\frac{E_{on} - E_{off}}{E_{off} I_0 F_A} \quad (2)$$

where n is the effective refractive index of the BHJ, c the speed of light in vacuum, ε_0 the vacuum dielectric constant, e the elementary charge, E_{on} the amplitude of the THz field at the maximum of the THz waveform, as transmitted through the photoexcited sample, and E_{off} the amplitude of the THz field at the maximum of the THz waveform, as transmitted through the sample in the ground state. The effective terahertz refractive index is calculated by Maxwell–Garnett theory,[34] where the volume-weighted average over the different constituent components is used for the medium refractive index, and the bulk optical refractive index is used for the QDs.

Steady-State Absorption. See Supporting Information, Note 1, for details.

Photoluminescence Spectroscopy. See Supporting Information, Note 1, for details.

Conflict of Interest: The authors declare no competing financial interest. S.T.C. performed the synthesis and experiments, analyzed the data, and wrote the manuscript. J.M.S. designed the ultrafast spectroscopy experiments and commented on the experimental and analytical work. L.D.A.S. designed the project and edited the manuscript. All authors discussed the results and implications and commented on the manuscript at all stages.

Acknowledgment. We thank D. Murthy, T. Savenije, A. Houtepen, L. Kunneman, S. Böhme, and H. Guo for discussions. This work is part of the Joint Solar Programme (JSP) of the Stichting voor Fundamenteel Onderzoek der Materie FOM, which is supported financially by the Nederlandse Organisatie voor Wetenschappelijk Onderzoek (NWO). This work is cofinanced by Nuon Helianthos.

Supporting Information Available: Absorption and photoluminescence spectra; calculation of the fraction of absorbed light; list of chemicals used. This material is available free of charge *via* the Internet at http://pubs.acs.org.

REFERENCES AND NOTES

1. Xue, J. G. Perspectives on Organic Photovoltaics. *Polym. Rev.* **2010**, *50*, 411–419.
2. Clarke, T. M.; Durrant, J. R. Charge Photogeneration in Organic Solar Cells. *Chem. Rev.* **2010**, *110*, 6736–6767.
3. Liang, Y. Y.; Yu, L. P. Development of Semiconducting Polymers for Solar Energy Harvesting. *Polym. Rev.* **2010**, *50*, 454–473.
4. Anthony, J. E. Small-Molecule, Nonfullerene Acceptors for Polymer Bulk Heterojunction Organic Photovoltaics. *Chem. Mater.* **2011**, *23*, 583–590.
5. Jasieniak, J.; Califano, M.; Watkins, S. E. Size-Dependent Valence and Conduction Band-Edge Energies of Semiconductor Nanocrystals. *ACS Nano* **2011**, *5*, 5888–5902.
6. Itskos, G.; Othonos, A.; Rauch, T.; Tedde, S. F.; Hayden, O.; Kovalenko, M. V.; Heiss, W.; Choulis, S. A. Optical Properties of Organic Semiconductor Blends with Near-Infrared Quantum-Dot Sensitizers for Light Harvesting Applications. *Adv. Energy Mater.* **2011**, *1*, 802–812.
7. Jarzab, D.; Szendrei, K.; Yarema, M.; Pichler, S.; Heiss, W.; Loi, M. A. Charge-Separation Dynamics in Inorganic-Organic Ternary Blends for Efficient Infrared Photodiodes. *Adv. Funct. Mater.* **2011**, *21*, 1988–1992.
8. Sargent, E. H. Infrared Photovoltaics Made by Solution Processing. *Nat. Photonics* **2009**, *3*, 325–331.
9. Dayal, S.; Reese, M. O.; Ferguson, A. J.; Ginley, D. S.; Rumbles, G.; Kopidakis, N. The Effect of Nanoparticle Shape on the Photocarrier Dynamics and Photovoltaic Device Performance of Poly(3-Hexylthiophene):CdSe Nanoparticle Bulk Heterojunction Solar Cells. *Adv. Funct. Mater.* **2010**, *20*, 2629–5264.
10. Chen, H. Y.; Hou, J. H.; Dayal, S.; Huo, L. J.; Kopidakis, N.; Beard, M. C.; Luther, J. M. A P-Type Quantum Dot/Organic Donor:Acceptor Solar-Cell Structure for Extended Spectral Response. *Adv. Energy Mater.* **2011**, *1*, 528–533.
11. Talgorn, E.; Gao, Y. N.; Aerts, M.; Kunneman, L. T.; Schins, J. M.; Savenije, T. J.; van Huis, M. A.; van der Zant, H. S. J.; Houtepen, A. J.; Siebbeles, L. D. A. Unity Quantum Yield of

Photogenerated Charges and Band-Like Transport in Quantum-Dot Solids. *Nat. Nanotechnol.* **2011**, *6*, 733–739.
12. Beard, M. C.; Turner, G. M.; Schmuttenmaer, C. A. Transient Photoconductivity in GaAs as Measured by Time-Resolved Terahertz Spectroscopy. *Phys. Rev. B* **2000**, *62*, 15764–15777.
13. Ulbricht, R.; Hendry, E.; Shan, J.; Heinz, T. F.; Bonn, M. Carrier Dynamics in Semiconductors Studied with Time-Resolved Terahertz Spectroscopy. *Rev. Mod. Phys.* **2011**, *83*, 543.
14. Rauch, T.; Boberl, M.; Tedde, S. F.; Furst, J.; Kovalenko, M. V.; Hesser, G. N.; Lemmer, U.; Heiss, W.; Hayden, O. Near-Infrared Imaging with Quantum-Dot-Sensitized Organic Photodiodes. *Nat. Photonics* **2009**, *3*, 332–336.
15. Gocalińska, A.; Saba, M.; Quochi, F.; Marceddu, M.; Szendrei, K.; Gao, J.; Loi, M. A.; Yarema, M.; Seyrkammer, R.; Heiss, W.; *et al*. Size-Dependent Electron Transfer from Colloidal PbS Nanocrystals to Fullerene. *J. Phys. Chem. Lett.* **2010**, *1*, 1149–1154.
16. Yang, Y.; Rodriguez-Cordoba, W.; Lian, T. Q. Ultrafast Charge Separation and Recombination Dynamics in Lead Sulfide Quantum Dot-Methylene Blue Complexes Probed by Electron and Hole Intraband Transitions. *J. Am. Chem. Soc.* **2011**, *133*, 9246–9249.
17. Parkinson, P.; Lloyd-Hughes, J.; Johnston, M. B.; Herz, L. M. Efficient Generation of Charges *via* Below-Gap Photoexcitation of Polymer-Fullerene Blend Films Investigated by Terahertz Spectroscopy. *Phys. Rev. B* **2008**, *78*, 115321.
18. Guo, J. M.; Ohkita, H.; Benten, H.; Ito, S. Charge Generation and Recombination Dynamics in Poly(3-Hexylthiophene)/Fullerene Blend Films with Different Regioregularities and Morphologies. *J. Am. Chem. Soc.* **2010**, *132*, 6154–6164.
19. Heath, G. A.; Mcgrady, J. E.; Martin, R. L. Characterization of the UV, Visible and Near-IR Spectra of the Fulleride Anions C_{60}^{1-}, C_{60}^{2-} and C_{60}^{3-}, and Theoretical Analysis of the Spectra of C_{60}^{1+}, C_{60}^{0}, C_{60}^{1-}, C_{60}^{2-} and C_{60}^{3-} by Self Consistent Field-Xα-Scattered-Wave (SCF-Xα-SW) Calculations. *J. Chem. Soc., Chem. Commun.* **1992**, *17*, 1272–1274.
20. Piris, J.; Dykstra, T. E.; Bakulin, A. A.; van Loosdrecht, P. H. M.; Knulst, W.; Trinh, M. T.; Schins, J. M.; Siebbeles, L. D. A. Photogeneration and Ultrafast Dynamics of Excitons and Charges in P3HT/PCBM Blends. *J. Phys. Chem. C* **2009**, *113*, 14500–14506.
21. Marcus, R. A. On the Theory of Oxidation-Reduction Reactions Involving Electron Transfer. I. *J. Chem. Phys.* **1956**, *24*, 966–978.
22. Imahori, H.; Tkachenko, N. V.; Vehmanen, V.; Tamaki, K.; Lemmetyinen, H.; Sakata, Y.; Fukuzumi, S. An Extremely Small Reorganization Energy of Electron Transfer in Porphyrin-Fullerene Dyad. *J. Phys. Chem. A* **2001**, *105*, 1750–1756.
23. Grozema, F. C.; Siebbeles, L. D. A. Mechanism of Charge Transport in Self-Organizing Organic Materials. *Int. Rev. Phys. Chem.* **2008**, *27*, 87–138.
24. Maria, A.; Cyr, P. W.; Klern, E. J. D.; Levina, L.; Sargent, E. H. Solution-Processed Infrared Photovoltaic Devices with >10% Monochromatic Internal Quantum Efficiency. *Appl. Phys. Lett.* **2005**, *87*, 213112.
25. Hayden, L. M.; Cunningham, P. D. Carrier Dynamics Resulting from Above and Below Gap Excitation of P3HT and P3HT/PCBM Investigated by Optical-Pump Terahertz-Probe Spectroscopy. *J. Phys. Chem. C* **2008**, *112*, 7928–7935.
26. Grzegorczyk, W. J.; Savenije, T. J.; Dykstra, T. E.; Piris, J.; Schins, J. M.; Siebbeles, L. D. A. Temperature-Independent Charge Carrier Photogeneration in P3HT-PCBM Blends with Different Morphology. *J. Phys. Chem. C* **2010**, *114*, 5182–10368.
27. Murthy, D. H. K.; Gao, M.; Vermeulen, M. J. W.; Siebbeles, L. D. A.; Savenije, T. J. Mechanism of Mobile Charge Carrier Generation in Blends of Conjugated Polymers and Fullerenes: Significance of Charge Delocalization and Excess Free Energy. *J. Phys. Chem. C* **2012**, *116*, 9214–9220.
28. Ferguson, A. J.; Kopidakis, N.; Shaheen, S. E.; Rumbles, G. Dark Carriers, Trapping, and Activation Control of Carrier Recombination in Neat P3HT and P3HT:PCBM Blends. *J. Phys. Chem. C* **2011**, *115*, 23134–23148.
29. Li, Z.; Gao, F.; Greenham, N. C.; McNeill, C. R. Comparison of the Operation of Polymer/Fullerene, Polymer/Polymer, and Polymer/Nanocrystal Solar Cells: A Transient Photocurrent and Photovoltage Study. *Adv. Funct. Mater.* **2011**, *21*, 1419–2850.
30. Konstantatos, G.; Clifford, J.; Levina, L.; Sargent, E. H. Sensitive Solution-Processed Visible-Wavelength Photodetectors. *Nat. Photonics* **2007**, *1*, 531–534.
31. Scholes, G. D.; Hines, M. A. Colloidal PbS Nanocrystals with Size-Tunable Near-Infrared Emission: Observation of Post-Synthesis Self-Narrowing of the Particle Size Distribution. *Adv. Mater.* **2003**, *15*, 1844–1849.
32. Moreels, I.; Lambert, K.; Smeets, D.; De Muynck, D.; Nollet, T.; Martins, J. C.; Vanhaecke, F.; Vantomme, A.; Delerue, C.; Allan, G.; *et al*. Size-Dependent Optical Properties of Colloidal PbS Quantum Dots. *ACS Nano* **2009**, *3*, 3023–3030.
33. Murphy, J. E.; Beard, M. C.; Nozik, A. J. Time-Resolved Photoconductivity of PbSe Nanocrystal Arrays. *J. Phys. Chem. B* **2006**, *110*, 25455–25461.
34. Choy, T. C. Effective Medium Theory. In *The International Series of Monographs on Physics*; Birman, J.; Edwards, S. F.; Friend, R. H.; Llewellyn-Smith, C. H.; Rees, M.; Sherrington, D.; Veneziano, G., Eds.; Clarendon Press: Oxford, 1999; pp 7−10.
35. Davis, R. J.; Lloyd, M. T.; Ferreira, S. R.; Bruzek, M. J.; Watkins, S. E.; Lindell, L.; Sehati, P.; Fahlman, M.; Anthony, J. E.; Hsu, J. W. P. Determination of Energy Level Alignment at Interfaces of Hybrid and Organic Solar Cells under Ambient Environment. *J. Mater. Chem.* **2011**, *21*, 1721–1729.
36. Savenije, T. J.; Kroeze, J. E.; Yang, X. N.; Loos, J. The Formation of Crystalline P3HT Fibrils upon Annealing of a PCBM:P3HT Bulk Heterojunction. *Thin Solid Films* **2006**, *511*, 2–6.
37. Tang, J.; Brzozowski, L.; Barkhouse, D.; Wang, X.; Debnath, R.; Wolowiec, R.; Palmiano, E.; Levina, L.; Pattantyus-Abraham, A.; Jamakosmanovic, D.; *et al*. Quantum Dot Photovoltaics in the Extreme Quantum Confinement Regime: The Surface-Chemical Origins of Exceptional Air- and Light-Stability. *ACS Nano* **2010**, *4*, 869–947.
38. Arbogast, J. W.; Darmanyan, A. P.; Foote, C. S.; Rubin, Y.; Diederich, F. N.; Alvarez, M. M.; Anz, S. J.; Whetten, R. L. Photophysical Properties of C_{60}. *J. Phys. Chem.* **1991**, *95*, 11–12.